

## Photoinduced PCET in Ruthenium–Phenol Systems: Thermodynamic Equivalence of Uni- and Bidirectional Reactions

Julia Nomrowski and Oliver S. Wenger\*

Department of Chemistry, University of Basel, St. Johannis-Ring 19, CH-4056 Basel, Switzerland

## Supporting Information

**ABSTRACT:** Six termolecular reaction systems comprised of  $\text{Ru}(4,4'\text{-bis(trifluoromethyl)-2,2'-bipyridine})_3^{2+}$ , phenols with different para substituents, and pyridine in acetonitrile undergo proton-coupled electron transfer (PCET) upon photoexcitation of the metal complex. Five of these six phenols are found to release in concerted fashion an electron to the ruthenium photooxidant and a proton to the pyridine base. The kinetics for this concerted bidirectional PCET process and its relationship to the reaction free energy were compared to the driving-force dependence of reaction kinetics for unidirectional concerted proton–electron transfer (CPET) between the same phenols and  $\text{Ru}(2,2'\text{-bipyrazine})_3^{2+}$ , a combined electron/proton acceptor. The results strongly support the concept of thermodynamic equivalence between separated electron/proton acceptors and single-reagent hydrogen-atom acceptors. A key feature of the explored systems is the similarity between molecules employed for bi- and unidirectional CPET.

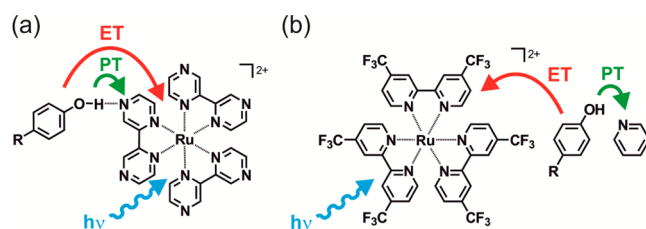
## INTRODUCTION

Proton-coupled electron transfer (PCET) can occur either in consecutive electron transfer (ET) and proton transfer (PT) steps (in whatever sequence) or in concerted fashion, that is, via a so-called concerted proton–electron transfer (CPET) mechanism.<sup>1</sup> A hallmark of the CPET mechanism is the avoidance of charged reaction intermediates, and therefore this process is often associated with significantly lower activation barriers than consecutive ET–PT or PT–ET mechanisms.<sup>2</sup>

So-called unidirectional PCET resembles hydrogen-atom transfer (HAT) in that the direction of electron and proton transfer is the same; that is, a combined electron/proton donor reacts with a combined electron/proton acceptor. In bidirectional PCET, also called multisite electron–proton transfer, more than two reaction partners are involved. A typical scenario is that a combined electron/proton donor releases its electron to an oxidant while its proton is transferred to a (separate) base. Phenols are a frequent choice as combined electron/proton donors because the phenolic proton becomes acidic upon oxidation.<sup>3</sup> Neutral phenols are not acidic in the solvents typically used for such studies, and consequently PT–ET mechanisms are less important. Moreover, O–H donors react at inherently faster rates than C–H donors.<sup>4</sup>

In recent years, there have been numerous mechanistic studies of uni- and bidirectional CPET,<sup>5</sup> and it has become clear that similar thermochemical considerations are useful for both reaction types.<sup>6</sup> However, the sets of reactants that are employed for experimental studies of unidirectional CPET are often very different from those used for investigations of bidirectional CPET. Here, we report results that permit a direct comparison of uni- and bidirectional CPET because the employed reactants are very similar in both reaction types.

In a prior study we found that unidirectional PCET between six different phenols and photoexcited  $\text{Ru}(\text{bpz})_3^{2+}$  ( $\text{bpz} = 2,2'\text{-bipyrazine}$ ) occurs predominantly via a CPET mechanism (Scheme 1a).<sup>7</sup> Here, we report on bidirectional CPET

Scheme 1<sup>a</sup>

<sup>a</sup>(a) Unidirectional CPET between phenols and photoexcited  $\text{Ru}(2,2'\text{-bipyrazine})_3^{2+}$  as investigated previously.<sup>7a</sup> (b) Bidirectional CPET between photoexcited  $\text{Ru}((\text{CF}_3)_2\text{bpy})_3^{2+}$ , phenols, and pyridine as investigated in this work. ET = electron transfer, PT = proton transfer.  $R = \text{OCH}_3, \text{CH}_3, \text{H}, \text{Cl}, \text{Br}, \text{CN}$ .

involving the same phenols as combined electron/proton donors, photoexcited  $\text{Ru}((\text{CF}_3)_2\text{bpy})_3^{2+}$  ( $(\text{CF}_3)_2\text{bpy} = 4,4'\text{-bis(trifluoromethyl)-2,2'-bipyridine}$ ) as an electron acceptor, and pyridine as a base (Scheme 1b). Change of the para substituents of the phenols ( $R\text{-PhOH}$ ) along the series  $R = \text{OCH}_3, \text{CH}_3, \text{H}, \text{Cl}, \text{Br}, \text{CN}$  permits systematic variation of the O–H bond dissociation free energy (BDFE) from 83.0 to 92.6 kcal/mol.<sup>3,8</sup>

Received: February 10, 2015

Published: March 17, 2015



**Table 1.** Electrochemical Potentials (in V vs  $\text{Fc}^+/\text{Fc}$ ) for One-Electron Oxidation of the Individual Phenols in  $\text{CH}_3\text{CN}$ ,  $\text{pK}_\text{a}$  Values of the Neutral Phenols in  $\text{CH}_3\text{CN}$ ,  $\text{pK}_\text{a}$  Values of the Respective Phenoxyl Radical Cations in  $\text{CH}_3\text{CN}$ , Experimental O–H Bond Dissociation Free Energies (BDFEs; in kcal/mol) in Dimethylsulfoxide, and Estimated BDFEs in  $\text{CH}_3\text{CN}$

R	$E(\text{R-PhOH}^+/0)^a$	$\text{pK}_\text{a}(\text{R-PhOH})$	$\text{pK}_\text{a}(\text{R-PhOH}^+)^b$	$\text{BDFE}_{\text{DMSO}}^d$	$\text{BDFE}_{\text{MeCN}}^e$
$\text{CH}_3\text{O}$	1.05	31.0 <sup>b</sup>	6.8	83.0	82.8
$\text{CH}_3$	1.16	27.5 <sup>c</sup>	8.4	87.1	86.3
H	1.25	26.6 <sup>c</sup>	4.8	88.3	88.3
Cl	1.25	25.4 <sup>c</sup>	1.5	88.7	88.3
Br	1.23	25.5 <sup>c</sup>	3.8	89.1	89.1
CN	1.40	22.7 <sup>c</sup>	−0.4	92.6	92.7

<sup>a</sup>From ref 10. <sup>b</sup>Calculated on the basis of  $\text{pK}_\text{a}$  values for DMSO reported in refs 3 and 8 using the procedure described in ref 11. <sup>c</sup>From ref 12.

<sup>d</sup>From refs 3 and 8. <sup>e</sup>Calculated for  $\text{CH}_3\text{CN}$  solution from gas-phase bond dissociation enthalpies as described in the text (see Supporting Information for details);<sup>8,13</sup> error bars are on the order of  $\pm 1.5$  kcal/mol.

## RESULTS AND DISCUSSION

**Simple Electron Transfer.** Photoexcited  $\text{Ru}((\text{CF}_3)_2\text{bpy})_3^{2+}$  in  $\text{CH}_3\text{CN}$  is a rather strong oxidant with a reduction potential of 0.9 V versus  $\text{Fc}^+/\text{Fc}$  in its relatively long-lived  $^3\text{MLCT}$  excited state.<sup>9</sup> However, in  $\text{CH}_3\text{CN}$  the six phenols from Scheme 1 are all oxidized at even more positive potentials (Table 1).<sup>10</sup>

Consequently, five of the six considered phenols are unable to quench the  $^3\text{MLCT}$  luminescence emitted by  $\text{Ru}((\text{CF}_3)_2\text{bpy})_3^{2+}$  in pure  $\text{CH}_3\text{CN}$ . Only 4-methoxyphenol ( $\text{CH}_3\text{O-PhOH}$ ) is a sufficiently strong electron donor to induce some detectable luminescence quenching by photo-induced electron transfer (Supporting Information, Figure S1). Stern–Volmer analysis of steady-state and time-resolved luminescence data (Supporting Information, Figure S2) leads to the conclusion that the rate constant for bimolecular electron transfer from  $\text{CH}_3\text{O-PhOH}$  to photoexcited  $\text{Ru}((\text{CF}_3)_2\text{bpy})_3^{2+}$  is  $k_{\text{ET}} = (6.95 \pm 0.17) \times 10^7 \text{ M}^{-1} \text{ s}^{-1}$  in  $\text{CH}_3\text{CN}$  at 20 °C. As far as the five other phenols are concerned, given a  $^3\text{MLCT}$  lifetime of  $\sim 580$  ns for  $\text{Ru}((\text{CF}_3)_2\text{bpy})_3^{2+}$  in aerated  $\text{CH}_3\text{CN}$  and the lack of any detectable luminescence quenching for phenol concentrations of up to 0.55 M (in absence of any base), one can conclude that the upper limit of  $k_{\text{ET}}$  for the phenols with  $\text{R} = \text{CH}_3, \text{H}, \text{Cl}, \text{Br}, \text{CN}$  is  $1 \times 10^5 \text{ M}^{-1} \text{ s}^{-1}$ . In other words, simple (i.e., not proton-coupled) electron transfer is inefficient for all phenols except 4-methoxyphenol. For the latter it is moderately efficient.

**Photochemistry in the Presence of Pyridine.** When pyridine is present in  $\text{CH}_3\text{CN}$ , phenol concentrations on the order of 0.3 M lead to readily detectable  $^3\text{MLCT}$  luminescence quenching in all six cases. This is exemplified by the luminescence data obtained with  $\text{CH}_3\text{-PhOH}$  shown in Figure 1. Analogous data for the five other phenol/ruthenium reaction couples can be found in the Supporting Information (Figures S3–S7). Figure 1a shows steady-state luminescence spectra obtained from aerated  $\text{CH}_3\text{CN}$  solutions containing  $\text{Ru}((\text{CF}_3)_2\text{bpy})_3^{2+}$  ( $2 \times 10^{-5} \text{ M}$ ) in the presence of a fixed concentration of  $\text{CH}_3\text{-PhOH}$  (42 mM) but variable pyridine concentrations (see inset). Excitation occurred at 450 nm, that is, selectively into the  $^1\text{MLCT}$  absorption band of  $\text{Ru}((\text{CF}_3)_2\text{bpy})_3^{2+}$ . As the pyridine concentration increases from 0 to 1.23 M, the  $\text{Ru}((\text{CF}_3)_2\text{bpy})_3^{2+}$   $^3\text{MLCT}$  luminescence intensity decreases by roughly 20%. The  $^3\text{MLCT}$  luminescence lifetime (measured after pulsed excitation at 532 nm) decreases from 580 ns in pure aerated  $\text{CH}_3\text{CN}$  to 460 ns in the presence of 1.23 M pyridine, that is, the lifetime shortens by 21%. In a control experiment with  $2 \times 10^{-5} \text{ M}$   $\text{Ru}((\text{CF}_3)_2\text{bpy})_3^{2+}$  in  $\text{CH}_3\text{CN}$  and pyridine concentrations varying between 0 and 1.0

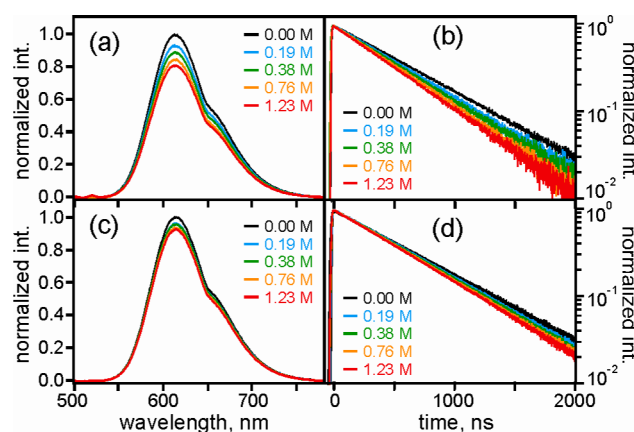


**Figure 1.** (a) Steady-state luminescence spectra obtained from aerated  $\text{CH}_3\text{CN}$  solutions containing  $\text{Ru}((\text{CF}_3)_2\text{bpy})_3^{2+}$  ( $2 \times 10^{-5} \text{ M}$ ) in the presence of a fixed concentration of  $\text{CH}_3\text{-PhOH}$  (42 mM) but variable pyridine concentrations (see inset); (b) luminescence decays detected at 610 nm after excitation of the same solutions at 532 nm with laser pulses of  $\sim 10$  ns duration. (c) Experiments analogous to those in (a) but with  $\text{CH}_3\text{-PhOD}$ ; (d) plot analogous to that of (b) but for  $\text{CH}_3\text{-PhOD}$ .

M but containing no phenol, the luminescence intensity does not decrease, and the luminescence lifetimes are unchanged (Supporting Information, Figure S8). Thus, it is clear that  $\text{CH}_3\text{-PhOH}$  and pyridine must be simultaneously present to quench the emission. The same is true for the phenols with  $\text{R} = \text{H}, \text{Cl}, \text{Br}, \text{CN}$ . For 4-methoxyphenol ( $\text{R} = \text{OCH}_3$ ) there is some emission quenching already in absence of pyridine as discussed above (Supporting Information, Figures S1 and S2), but pyridine addition at constant  $\text{CH}_3\text{O-PhOH}$  concentration makes emission quenching markedly more efficient (Supporting Information, Figure S3). Thus, for all six phenols the presence of pyridine is crucial for inducing substantial  $\text{Ru}((\text{CF}_3)_2\text{bpy})_3^{2+}$  luminescence quenching.

Phenols form hydrogen bonds to pyridine in aprotic solution.<sup>5a,j,14</sup> Hydrogen-bonded phenols in turn are known to have markedly less positive oxidation potentials than non-hydrogen-bonded phenols because electron release is coupled to deprotonation. In other words, phenol oxidation in the presence of proton acceptors is a PCET process.<sup>2a,5b,15</sup> It has been demonstrated that the lowering of the oxidation potentials is so substantial that this effect can only be satisfactorily explained in terms of a CPET mechanism.<sup>15</sup> The  $\text{Ru}((\text{CF}_3)_2\text{bpy})_3^{2+}$  luminescence quenching mentioned above for the six phenol/pyridine systems is the consequence of the lowering of the phenol oxidation potentials in the presence of

the proton acceptor pyridine. In fact, our experimental observations are conceptually analogous to those first made by Linschitz with triplet-excited  $C_{60}$  and hydrogen-bonded phenols.<sup>5a,14</sup>

Direct evidence for PCET photoproducts comes from transient absorption spectroscopy measured after selective  $Ru((CF_3)_2bpy)_3^{2+}$  excitation at 532 nm with laser pulses of  $\sim 10$  ns duration. An exemplary set of data, obtained from an aerated  $CH_3CN$  solution containing  $7 \times 10^{-5}$  M  $Ru((CF_3)_2bpy)_3^{2+}$ , 0.3 M  $CH_3-PhOH$ , and 1.0 M pyridine, is shown in Figure 2. The

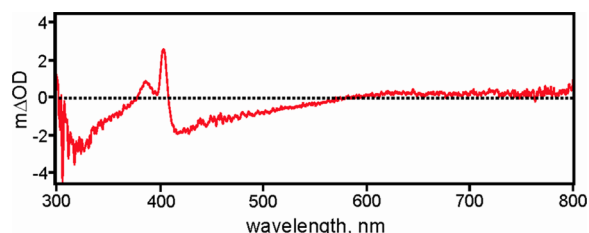
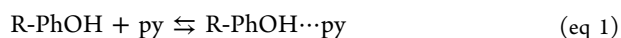


**Figure 2.** Transient difference spectrum obtained after excitation of an aerated  $CH_3CN$  solution containing  $7 \times 10^{-5}$  M  $Ru((CF_3)_2bpy)_3^{2+}$ , 0.3 mM  $CH_3-PhOH$ , and 1.0 M pyridine at 532 nm with laser pulses of  $\sim 10$  ns duration. Detection occurred by time-integration over an interval of 5  $\mu s$  starting 2  $\mu s$  after excitation.

absorption spectrum of 4-methylphenoxy radical ( $Me-PhO\cdot$ ) is observed with characteristic peaks at 404 and 386 nm;<sup>16</sup> the bleach around 430 nm is caused by disappearance of  $Ru((CF_3)_2bpy)_3^{2+}$   $^1MLCT$  absorption. Analogous transient absorption spectra were obtained for the five other phenol/pyridine combinations, in each case providing unambiguous evidence for the formation of charge-neutral phenoxy radicals (Supporting Information, Figure S9).<sup>16,17</sup> The latter are clearly the products of a photoinduced PCET reaction.

**Hydrogen-Bonding Equilibrium between Phenols and Pyridine.** In  $CH_3CN$  solution, there is chemical equilibrium between free phenol ( $R-PhOH$ ) and pyridine ( $py$ ) on one hand and hydrogen-bonded phenol–pyridine adducts ( $R-PhOH\cdots py$ ) on the other (eq 1).



Any quantitative analysis of the emission quenching data must take this equilibrium into account because only the hydrogen-bonded  $R-PhOH\cdots py$  adducts induce significant photoreaction for most phenols (see above). In a given solvent ( $CH_3CN$ ) at a given temperature (22 °C), the equilibrium (or association) constant ( $K_A$ ) is primarily a function of the phenol  $R$ -substituent.

One possibility to determine the equilibrium constant for the formation of hydrogen-bonded phenol–pyridine adducts is to make use of steady-state luminescence quenching data.<sup>5d,g</sup> However, this procedure leads to inconsistencies in the cases considered here. A method based on UV–vis absorption changes upon addition of large quantities of pyridine to dilute solutions of phenols as reported earlier turned out to be impractical in our cases, mainly due to mutual overlap of the absorption bands of phenol and pyridine.<sup>5a</sup> Consequently, the association constants between the various phenols and deuterated pyridine (pyridine- $d_5$ ) were determined by  $^1H$  NMR spectroscopy in  $CD_3CN$ .

In Figure 3a the  $^1H$  NMR spectrum of 25 mM  $CH_3-PhOH$  in  $CD_3CN$  at 22 °C is shown. The resonance of the phenolic proton under these conditions is at 6.64 ppm. With 25 mM (=

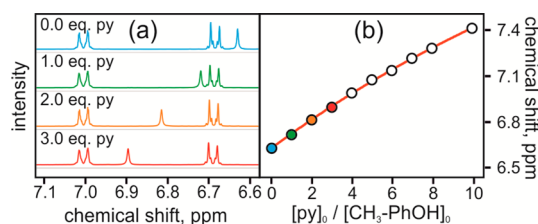


**Figure 3.** (a) Uppermost spectrum: Extract of the  $^1H$  NMR spectrum of a 25 mM solution of  $CH_3-PhOH$  in  $CD_3CN$  at 22 °C. Spectra of the same solution with 1, 2, and 3 equiv of pyridine- $d_5$  present are shown below. (b) Chemical shift of the O–H resonance as a function of pyridine- $d_5$  concentration in ppm; data extracted from (a) and Supporting Information, Figure S11.  $[py]_0$  is the nominal pyridine- $d_5$  concentration,  $[CH_3-PhOH]_0$  is the nominal 4-methylphenol concentration; the latter was kept constant at 25 mM throughout the NMR titration experiment.

1 equiv) pyridine- $d_5$  present the O–H resonance shifts to 6.72 ppm, and when increasing the pyridine concentration further, the respective signal is shifted further downfield. The chemical shift of the O–H resonance in  $CD_3CN$  at 22 °C as a function of pyridine concentration (while keeping the  $CH_3-PhOH$  concentration constant) is shown in Figure 3b. The solid line in Figure 3b is the result of a fit to the NMR titration data in the so-called fast-exchange limit, see Supporting Information for further details.<sup>18</sup> An association constant of  $1.1 \pm 0.1$  M $^{-1}$  is determined for  $CH_3-PhOH$  and pyridine- $d_5$  in  $CD_3CN$  at 22 °C (Table 2). Analogous  $^1H$  NMR titrations with the five other

**Table 2.** Equilibrium Constants for Formation of Hydrogen-Bonded Phenol–Pyridine- $d_5$  Adducts in  $CD_3CN$  at 22 °C ( $K_A$ , eq 1) Determined from  $^1H$  NMR Titration Experiments with Pyridine- $d_5$  (Supporting Information, Figure S10–S16). Abraham's Hydrogen Bonding Parameters ( $\alpha_2^H$ ) for Phenols<sup>19</sup>

R	$K_A$ [M $^{-1}$ ]	$\alpha_2^H$
OCH <sub>3</sub>	$1.2 \pm 0.1$	0.550
CH <sub>3</sub>	$1.1 \pm 0.1$	0.571 <sup>a</sup>
H	$1.1 \pm 0.1$	0.596
Cl	$1.5 \pm 0.1$	0.670
Br	$1.4 \pm 0.1$	0.674
CN	$2.1 \pm 0.1$	0.787

<sup>a</sup>Value for 4-(*tert*-butyl)phenol taken as an approximation for the unknown value of  $CH_3-PhOH$ .

phenols (Supporting Information, Figures S10–S15) produced the  $K_A$  values reported in Table 2 (Supporting Information, Figure S16); the error bars correspond to the standard deviations resulting from the fits to the experimental data.

The association constants in Table 2 are found to increase with increasing hydrogen-bond donor ability of the involved phenol. The hydrogen-bond donor ability is captured by Abraham's hydrogen-bonding parameters ( $\alpha_2^H$ ) given in the last column of Table 2.<sup>19</sup>

**Determination of Rate Constants for Concerted Proton–Electron Transfer.** The steady-state luminescence quenchings such as those shown in Figure 1a are accompanied by a shortening of the luminescence lifetime. The data in Figure 4a were measured using aerated  $CH_3CN$  solutions containing  $2 \times 10^{-5}$  M  $Ru((CF_3)_2bpy)_3^{2+}$ , 42 mM  $CH_3-PhOH$ , and pyridine concentrations ranging from 0 to 1.9 M (see inset); that is, these are the same solutions as those employed for obtaining



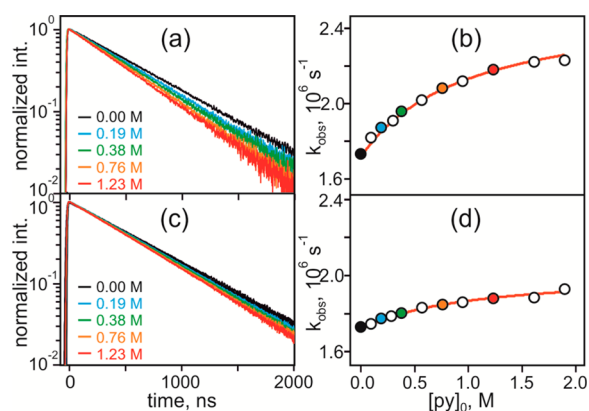


**Figure 4.** (a)  $^3\text{MLCT}$  luminescence decays measured after excitation of an aerated  $\text{CH}_3\text{CN}$  solution containing  $\text{Ru}((\text{CF}_3)_2\text{bpy})_3^{2+}$  ( $2 \times 10^{-5}$  M) in the presence of a fixed concentration of  $\text{CH}_3\text{-PhOH}$  (42 mM) and variable pyridine concentrations (see inset); same data as in Figure 1b. Excitation occurred at 532 nm with pulses of  $\sim 10$  ns duration, detection was at 610 nm; (b) plot of excited-state decay rate constants ( $k_{\text{obs}}$ ) extracted from the  $^3\text{MLCT}$  luminescence decays in (a) (and from additional decay data not included in (a)) as a function of nominal pyridine concentration; the  $\text{CH}_3\text{-PhOH}$  concentration was 42 mM. (c) Same experiment as in (a) but with deuterated 4-methylphenol ( $\text{CH}_3\text{-PhOD}$ ); same data as in Figure 1d; (d) plot based on the lifetime data from (c) for which deuterated 4-methylphenol ( $\text{CH}_3\text{-PhOD}$ ) was used.

the data from Figure 1a. Analogous experiments, making use of 532 nm laser excitation pulses of  $\sim 10$  ns duration, were performed for the five other phenol/pyridine couples, and the respective data are given in the Supporting Information (Figures S17–S21). All luminescence decays are single exponential over at least 2 orders of magnitude, and decay rate constants ( $k_{\text{obs}}$ ) were extracted from monoexponential fits to the experimental decay data. We recall that addition of up to 1 M pyridine to  $2 \times 10^{-5}$  M solutions of  $\text{Ru}((\text{CF}_3)_2\text{bpy})_3^{2+}$  in aerated  $\text{CH}_3\text{CN}$  does not lead to any changes in luminescence lifetime (Supporting Information, Figure S8b). Figure 4b contains a plot of  $k_{\text{obs}}$  versus pyridine concentration for the  $\text{CH}_3\text{-PhOH}$ /pyridine system. Analogous plots for the five other phenol/pyridine couples can be found in the Supporting Information (Figures S17–S21).

For all six phenol/pyridine combinations, the observed  $\text{Ru}((\text{CF}_3)_2\text{bpy})_3^{2+}$  luminescence decay rate constants ( $k_{\text{obs}}$ ) are a function of the intrinsic  $^3\text{MLCT}$  excited-state decay ( $k_0$ ), the excited-state decay caused by simple (i.e., not proton-coupled) electron transfer to the phenols ( $k_{\text{ET}}$ ), and the contribution to excited-state quenching via CPET involving hydrogen-bonded phenol–pyridine adducts ( $k_{\text{CPET}}$ ) as reflected by the three summands appearing in eq 2.<sup>5a,g,14</sup>

$$k_{\text{obs}} = k_0 + k_{\text{ET}} \times [\text{R-PhOH}] + k_{\text{CPET}} \times [\text{R-PhOH} \cdots \text{py}] \quad (\text{eq } 2)$$

The intrinsic excited-state decay rate constant ( $k_0$ ) is readily available from a luminescence lifetime measurement of  $2 \times 10^{-5}$  M  $\text{Ru}((\text{CF}_3)_2\text{bpy})_3^{2+}$  in pure aerated  $\text{CH}_3\text{CN}$ . This experiment yields  $k_0 \approx 1.72 \times 10^6 \text{ s}^{-1}$  (Supporting Information, Figure S8b). As noted above, for the phenols with  $\text{R} = \text{CH}_3$ , H, Cl, Br, and CN, the rate constant  $k_{\text{ET}}$  is smaller than  $1 \times 10^5 \text{ M}^{-1} \text{ s}^{-1}$ , and the nominal phenol concentrations are 0.3 M or lower. Consequently, the  $k_{\text{ET}} \times [\text{R-PhOH}]$  term only plays an important role for 4-methoxyphenol, for which we have found

$k_{\text{ET}} = (6.95 \pm 0.17) \times 10^7 \text{ M}^{-1} \text{ s}^{-1}$  (see above). For the five other phenols the middle term in eq 2 can be neglected.

The  $k_{\text{CPET}} \times [\text{R-PhOH} \cdots \text{py}]$  term of eq 2 accounts for the dependence of  $k_{\text{obs}}$  on the pyridine concentration. As described in detail in the Supporting Information,  $k_{\text{obs}}$  can be expressed as a function of the nominal phenol and pyridine concentrations (eq 3).<sup>5a,d,g,14</sup> Note that eq 3 is only an approximation because a  $[\text{R-PhOH} \cdots \text{py}]^2$  summand was neglected in the denominator of the last term; see Supporting Information for details.

$$k_{\text{obs}} \approx k_0 + k_{\text{ET}} \times [\text{R-PhOH}]_0 + (k_{\text{CPET}} - k_{\text{ET}}) \times \frac{K_A \times [\text{R-PhOH}]_0 \times [\text{py}]_0}{1 + K_A \times [\text{py}]_0 + K_A \times [\text{R-PhOH}]_0} \quad (\text{eq } 3)$$

The solid red lines in Figure 4 are the result of fits with eq 3 to the experimental  $k_{\text{obs}}$  versus pyridine concentration data using  $k_{\text{CPET}}$  as the only adjustable parameter. For these fits,  $k_0$  was set to  $1.72 \times 10^6 \text{ s}^{-1}$ ,  $k_{\text{ET}} = 0 \text{ M}^{-1} \text{ s}^{-1}$  (the  $k_{\text{ET}} \times [\text{R-PhOH}]_0$  term can be neglected for  $\text{CH}_3\text{-PhOH}$  for reasons explained above),  $[\text{R-PhOH}]_0 = 0.042 \text{ M}$ , and  $K_A = 1.1 \text{ M}^{-1}$ , that is, the association constant determined above on the basis of the  $^1\text{H}$  NMR titration data (second column of Table 2). This procedure yields  $k_{\text{CPET}} = (1.98 \pm 0.19) \times 10^7 \text{ M}^{-1} \text{ s}^{-1}$  for  $\text{CH}_3\text{-PhOH}$  and  $(0.72 \pm 0.16) \times 10^7 \text{ M}^{-1} \text{ s}^{-1}$  for  $\text{CH}_3\text{-PhOD}$ , respectively; the error bars correspond to standard deviations of the fits with eq 3; the experimental uncertainty associated with the determination of  $k_{\text{obs}}$  is 5%. Table 3 lists the  $k_{\text{CPET}}$  values

**Table 3.** Rate Constants for CPET between  $^3\text{MLCT}$ -Excited  $\text{Ru}((\text{CF}_3)_2\text{bpy})_3^{2+}$  and Phenol–Pyridine Adducts ( $k_{\text{CPET}}$ ) in  $\text{CH}_3\text{CN}$  at  $20^\circ\text{C}$ , Determined as Described in the Text

	R-PhOH	R-PhOD
R	$k_{\text{CPET}} [\text{M}^{-1} \text{ s}^{-1}]$	$k_{\text{CPET}} [\text{M}^{-1} \text{ s}^{-1}]$
OCH <sub>3</sub>	$(8.21 \pm 0.21) \times 10^8$	$(7.91 \pm 0.20) \times 10^8$
CH <sub>3</sub>	$(1.98 \pm 0.19) \times 10^7$	$(0.72 \pm 0.16) \times 10^7$
H	$(4.01 \pm 0.32) \times 10^6$	$(2.10 \pm 0.29) \times 10^6$
Cl	$(6.32 \pm 0.43) \times 10^6$	$(2.40 \pm 0.36) \times 10^6$
Br	$(4.99 \pm 0.41) \times 10^6$	$(1.25 \pm 0.34) \times 10^6$
CN	$(1.54 \pm 0.06) \times 10^7$	$(1.20 \pm 0.06) \times 10^7$

obtained from analogous one-parameter fits to the experimental data for all six phenol/pyridine combinations (Supporting Information, Figures S17–S21), using in each case the  $K_A$  values from Table 2 as nonadjustable input parameters as well as  $k_0 = 1.72 \times 10^6 \text{ s}^{-1}$  and  $k_{\text{ET}} = 0 \text{ M}^{-1} \text{ s}^{-1}$ , except for  $\text{CH}_3\text{O-PhOH}$ , for which  $k_{\text{ET}} = (6.95 \pm 0.17) \times 10^7 \text{ M}^{-1} \text{ s}^{-1}$  was used (see above). The resulting  $k_{\text{CPET}}$  values range from  $(1.25 \pm 0.34) \times 10^6 \text{ M}^{-1} \text{ s}^{-1}$  to  $(8.21 \pm 0.21) \times 10^8 \text{ M}^{-1} \text{ s}^{-1}$  (Table 3). This procedure and similar methods for determining  $k_{\text{CPET}}$  from time-resolved data have been employed earlier.<sup>5a,d,g,h,14,20</sup> Since the  $^1\text{H}$  NMR titration method from the previous section does not permit determination of association constants between deuterated phenols and pyridine, the  $K_A$  values from Table 2 were employed for both ordinary and deuterated phenols.

**H/D Kinetic Isotope Effects.** The occurrence of a significant H/D kinetic isotope effect (KIE) in the case of 4-methylphenol is evident already from the raw data in Figure 1. For any given pyridine concentration, the luminescence quenching in the presence of 42 mM  $\text{CH}_3\text{-PhOD}$  is weaker than in the presence of 42 mM  $\text{CH}_3\text{-PhOH}$ , and the luminescence lifetime is shortened less in the presence of 42

Table 4. H/D Kinetic Isotope Effects for PCET Reactions in the Systems from Scheme 1

R	OCH <sub>3</sub>	CH <sub>3</sub>	H	Cl	Br	CN
bidirectional <sup>a,b</sup>	1.0 ± 0.1	2.8 ± 0.7	1.9 ± 0.3	2.6 ± 0.4	4.0 ± 1.1	1.3 ± 0.1
unidirectional <sup>c,d</sup>	1.0 ± 0.1	1.7 ± 0.2	3.4 ± 0.2	7.8 ± 0.6	2.9 ± 0.2	10.2 ± 0.6

<sup>a</sup>For the systems from Scheme 1b. <sup>b</sup>Values correspond to the ratio of  $k_{\text{CPET}}$  values for ordinary and deuterated reactants from Table 3. <sup>c</sup>For the systems from Scheme 1a. <sup>d</sup>From ref 7a.

mM CH<sub>3</sub>-PhOD than in the presence of 42 mM CH<sub>3</sub>-PhOH. Quantitative analysis produces the H/D KIE values summarized in the upper row of Table 4. For comparison, the lower row of Table 4 summarizes the H/D KIEs determined previously for unidirectional CPET between the same six phenols and photoexcited Ru(bpz)<sub>3</sub><sup>2+</sup> (Scheme 1a).

In general KIEs depend on many different parameters, and the absence of a sizable H/D KIE is no argument against CPET, for example, because proton and deuteron transfer can proceed through different vibrational states.<sup>21</sup> We recall that the shift of phenol oxidation potentials in the presence of hydrogen-bond acceptors can only be satisfactorily explained by invoking CPET.<sup>15</sup> It seems likely that the PT distance has a decisive influence on the magnitude of the KIEs in our systems, as expected by theory and as suspected in other experimental PCET studies.<sup>2b,22</sup> The PT distance is certainly not identical for the unidirectional PCET reactions in Scheme 1a and the bidirectional PCET reactions in Scheme 1b. An explanation for the large deviation between H/D KIEs observed with 4-cyanophenol in the two types of settings (1.3 ± 0.1 vs 10.2 ± 0.6) will be given in the next section.

**Driving Force Dependence of Rate Constants for Concerted Proton–Electron Transfer.** For CPET between the reactants from Scheme 1b, the reaction free energy ( $\Delta G_{\text{CPET}}^0$ ) is basically the difference between the energetic cost associated with homolytic cleavage of the phenolic O–H bonds and the energetic gain associated with reduction of photoexcited Ru((CF<sub>3</sub>)<sub>2</sub>bpy)<sub>3</sub><sup>2+</sup> combined with protonation of pyridine. The O–H bond dissociation free energies (BDFEs) for the six phenols are known for dimethyl sulfoxide (DMSO) solution (fifth column of Table 1).<sup>3,8</sup> Alternatively, the O–H BDFEs in CH<sub>3</sub>CN solution can be estimated on the basis of (gas phase) bond dissociation enthalpies (BDEs) and Abraham's hydrogen bonding parameters as described previously.<sup>8,13a</sup> Using BDEs from the literature,<sup>13b</sup> the  $\alpha_2^{\text{H}}$  parameters from Table 2,<sup>19a</sup> and  $\beta_2^{\text{H}} = 0.44$  for CH<sub>3</sub>CN,<sup>8,13a</sup> one obtains the BDFEs reported in the last column of Table 1 (see Supporting Information for details). These values are remarkably close to the experimental BDFEs determined for DMSO solution, and this finding strongly supports our use of the latter for the following thermodynamic analyses.

Even though the electron and proton acceptors are separate molecules, a *formal* bond dissociation free energy (*f*BDFE) can be calculated for the Ru((CF<sub>3</sub>)<sub>2</sub>bpy)<sub>3</sub><sup>2+</sup>/pyridine couple using the standard reduction potential of the oxidant ( $E_{\text{red}}^0$ ) and the  $\text{p}K_{\text{a}}$  of the conjugate acid of the proton acceptor (eq 4).<sup>6</sup>

$$\begin{aligned} f\text{BDFE}(\text{X-H}) \text{ kcal/mol} \\ = 1.37 \times \text{p}K_{\text{a}} + 23.06 \times E_{\text{red}}^0 + C_{\text{G,CH}_3\text{CN}} \quad (\text{eq 4}) \end{aligned}$$

The last term in eq 4 is equivalent to the H<sup>+</sup>/H• standard reduction potential in CH<sub>3</sub>CN, and it includes the free energy for formation of H• as well as the free energy for solvation of H•.<sup>8</sup> For CH<sub>3</sub>CN at 298 K,  $C_{\text{G,CH}_3\text{CN}}$  is equal to 54.9 kcal/mol.<sup>8</sup> The reduction potential of the oxidant ( $E_{\text{red}}^0$ ) is to be used in

units of volts versus Fc<sup>+</sup>/Fc in CH<sub>3</sub>CN, and the  $\text{p}K_{\text{a}}$  value must be for CH<sub>3</sub>CN solution.<sup>6</sup> Using  $E_{\text{red}}^0 = 0.9$  V versus Fc<sup>+</sup>/Fc<sup>9</sup> and  $\text{p}K_{\text{a}} = 12.5$ ,<sup>23</sup> one obtains *f*BDFE = 93 kcal/mol. As noted before, the use of formal BDFEs may appear somewhat peculiar because no X–H bond is formed, but it has been proposed as a useful way to characterize the thermochemistry of a CPET system.<sup>6</sup> Several prior studies confirmed the usefulness of this concept,<sup>8,24</sup> but the systems from Scheme 1 are special in that the reactants used for unidirectional and bidirectional PCET are as similar as possible.

Thus, the CPET driving-force for the systems in Scheme 1b ( $\Delta G_{\text{CPET}}^0$ ) is the difference between the experimental O–H BDFEs for the six phenols from Table 1 and *f*BDFE = 93 kcal/mol, resulting in  $\Delta G_{\text{CPET}}^0$  values ranging from −10 kcal/mol (ca. −0.4 eV) to −0.4 kcal/mol (~0 eV). In our case CPET in CH<sub>3</sub>CN produces two monocations (Ru((CF<sub>3</sub>)<sub>2</sub>bpy)<sub>3</sub><sup>+</sup> and protonated pyridine) and a neutral species (phenoxyl radicals) out of a dication (photoexcited Ru((CF<sub>3</sub>)<sub>2</sub>bpy)<sub>3</sub><sup>2+</sup>) and two neutral molecules (phenols, pyridine). The solvation of the individual species may therefore be significantly different before and after CPET.

Figure 5a shows a semilogarithmic plot of  $k_{\text{CPET}}$  versus  $\Delta G_{\text{CPET}}^0$  for the six termolecular ruthenium/phenol/pyridine

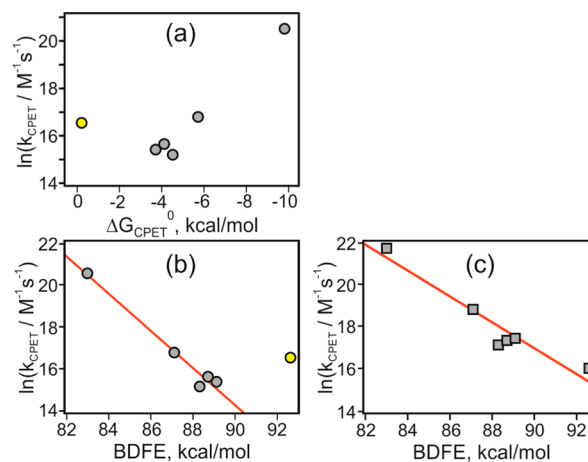


**Figure 5.** (a) Plot of  $\ln(k_{\text{CPET}}/\text{M}^{-1} \text{s}^{-1})$  vs  $\Delta G_{\text{CPET}}^0$  (in kcal/mol) for the termolecular reactions illustrated by Scheme 1b; (b) plot of  $\ln(k_{\text{CPET}}/\text{M}^{-1} \text{s}^{-1})$  vs O–H BDFEs for the termolecular reactions illustrated in Scheme 1b; (c) plot of  $\ln(k_{\text{CPET}}/\text{M}^{-1} \text{s}^{-1})$  vs O–H BDFEs for the bimolecular reactions illustrated by Scheme 1a.

reaction systems from Scheme 1b. For the phenols with R = OCH<sub>3</sub>, CH<sub>3</sub>, H, Cl, Br one recognizes a correlation between  $\ln(k_{\text{CPET}})$  and  $\Delta G_{\text{CPET}}^0$ , but 4-cyanophenol (yellow data point at  $\Delta G_{\text{CPET}}^0 = -0.4$  kcal/mol) stands out. The data in Figure 5a are compatible with CPET as a prevalent PCET reaction mechanism for all phenols except 4-cyanophenol.<sup>4,7b,8</sup>

The fact that CN-PhOH stands out is likely an indication for another PCET mechanism. A sequence of rate-determining electron transfer followed by rapid proton transfer (ET–PT)

seems highly unlikely based on the relevant redox potentials; initial ET from CN-PhOH to photoexcited  $\text{Ru}((\text{CF}_3)_2\text{bpy})_3^{2+}$  is expected to be endergonic by 0.5 eV (Table 1). The only alternative is then a sequential PT–ET mechanism in which an initial PT step is followed by rapid ET. CN-PhOH is the most acidic of the six phenols considered in this work, and based on  $\text{pK}_a$  values of 22.7 for CN-PhOH and 12.5 for pyridinium in  $\text{CH}_3\text{CN}$ , we estimate that under the experimental conditions used for the luminescence quenching studies up to  $\sim 4 \mu\text{M}$  4-cyanophenolate ( $\text{CN-PhO}^-$ ) is present. The latter is a strong reductant with  $E_{\text{ox}} = 0.15 \text{ V}$  versus  $\text{Fc}^+/\text{Fc}$  in DMSO and can therefore be expected to quench the  $^3\text{MLCT}$  excited state of  $\text{Ru}((\text{CF}_3)_2\text{bpy})_3^{2+}$  with a diffusion-limited rate constant. We attempted fits to the experimental data with an extended version of eq 3 containing an additional summand ( $k_{\text{diff}} \times [\text{R-PhO}^-]$ ) reflecting diffusion-limited ( $k_{\text{diff}} = 1.9 \times 10^{10} \text{ M}^{-1} \text{ s}^{-1}$  for  $\text{CH}_3\text{CN}$ )<sup>25</sup> reductive excited-state quenching by 4-cyanophenolate; the concentration of the latter was calculated on the basis of  $[\text{CN-PhOH}]_0 = 0.15 \text{ M}$ ,  $[\text{py}]_0 = 0\text{--}2.0 \text{ M}$ , and the above-mentioned  $\text{pK}_a$  values. However, these fits do not provide satisfactory results, possibly because of uncertainties in the acidity constants of 4-cyanophenol and pyridinium in  $\text{CH}_3\text{CN}$ . Yet it seems plausible that the rate constant given for CN-PhOH in Table 3 does not reflect CPET kinetics but rather reflects reaction of a small fraction of 4-cyanophenolate, which is formed in a PT pre-equilibrium. The comparatively small H/D KIE of  $1.3 \pm 0.1$  is in line with this interpretation.

**Comparison between Bi- and Unidirectional Concerted Proton–Electron Transfer.** Figure 5b plots  $\ln(k_{\text{CPET}})$  versus O–H BDFEs for the termolecular reactions illustrated in Scheme 1b, and this is merely another representation of the data from Figure 5a. It permits direct comparison with analogous data obtained for the reaction pairs from Scheme 1a in which the same six phenols undergo unidirectional CPET with photoexcited  $\text{Ru}(\text{bpz})_3^{2+}$ , a combined electron–proton acceptor requiring no addition of pyridine base.<sup>7</sup> For photoexcited  $\text{Ru}(\text{bpz})_3^{2+}$  the relevant N–H BDFEs (for hydrogen-atom binding to the N atoms of the bpz ligand periphery) could not be determined, and therefore in this case  $k_{\text{CPET}}$  can only be plotted as a function of phenol O–H BDFEs. The correlations in Figure 5b,c (red lines) are typical for hydrogen-atom transfer (HAT) reactions as first discussed by Evans and Polanyi.<sup>4,26</sup> Thus, bi- and unidirectional CPET with the same set of phenols exhibit a very similar dependence of reaction rates on free energies. The only exception is 4-cyanophenol in the data set of Figure 5b, for reasons discussed above. In the studies of unidirectional (HAT-like) PCET between phenols and photoexcited  $\text{Ru}(\text{bpz})_3^{2+}$ , the 4-cyanophenol data point matches the correlation between  $\ln(k_{\text{CPET}})$  and O–H BDFE well (Figure 5c).<sup>7</sup> The important difference from the investigations of bidirectional PCET with the termolecular phenol/ $\text{Ru}((\text{CF}_3)_2\text{bpy})_3^{2+}$ /pyridine reaction systems is that in the earlier studies of unidirectional PCET with  $\text{Ru}(\text{bpz})_3^{2+}$  there is no pyridine which can lead to the formation of a non-negligible amount of 4-cyanophenolate.<sup>7a</sup>

Using the Eyring equation it is possible to estimate activation free energies ( $\Delta G_{\text{CPET}}^\ddagger$ ) for the CPET processes based on the reaction rate constants ( $k_{\text{CPET}}$ ) from Table 3. Using a prefactor of  $Z = 1 \times 10^{11} \text{ M}^{-1} \text{ s}^{-1}$  in the Eyring equation, one obtains  $\Delta G_{\text{CPET}}^\ddagger$  values ranging from  $2.8 \pm 0.3 \text{ kcal/mol}$  for  $\text{CH}_3\text{O-PhOH}$  to  $5.9 \pm 0.6 \text{ kcal/mol}$  for  $\text{H-PhOH}$ .<sup>27</sup> The respective activation free energies are plotted against the phenol O–H BDFEs in Figure 6a. An analogous plot of  $\Delta G_{\text{CPET}}^\ddagger$  values versus

phenol O–H BDFEs based on data for unidirectional CPET between the reaction pairs from Scheme 1a is shown in Figure 6b.<sup>7a</sup>

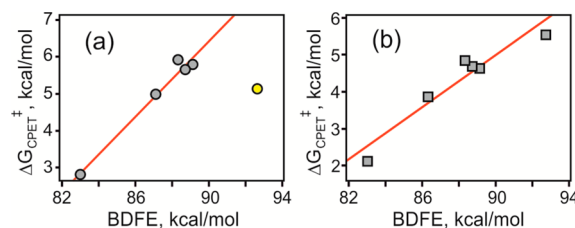


**Figure 6.** (a) Plot of activation free energies (estimated on the basis of the  $k_{\text{CPET}}$  values from Table 3 and the Eyring equation with a prefactor of  $Z = 1 \times 10^{11} \text{ M}^{-1} \text{ s}^{-1}$ ) vs O–H BDFEs for the termolecular reactions systems from Scheme 1b; (b) analogous plot for the bimolecular reactions systems from Scheme 1a.<sup>7a</sup>

$\Delta G_{\text{CPET}}^\ddagger$  is experimentally more accurately accessible by measurement of the temperature dependence of the termolecular CPET reactions. Figure 7 contains a plot of

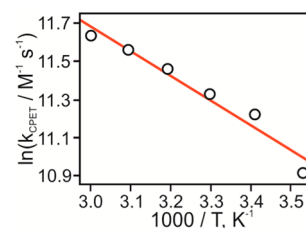


**Figure 7.** Plot of  $\ln(k_{\text{CPET}})$  against inverse temperature for the termolecular reaction between photoexcited  $\text{Ru}((\text{CF}_3)_2\text{bpy})_3^{2+}$ ,  $\text{CH}_3\text{-PhOH}$ , and pyridine in  $\text{CH}_3\text{CN}$ .

$\ln(k_{\text{CPET}})$  versus inverse temperature for the reaction with  $\text{CH}_3\text{-PhOH}$ . For the purpose of acquiring the relevant experimental data, sets of time-resolved luminescence data as illustrated in Figure 4 were acquired at six different temperatures, and  $k_{\text{CPET}}$  was determined for each temperature based on the  $K_A$  value obtained from  $^1\text{H}$  NMR titrations at  $22^\circ\text{C}$ . Using the Eyring equation (in combination with the relationship  $\Delta G_{\text{CPET}}^\ddagger = \Delta H_{\text{CPET}}^\ddagger - T \times \Delta S_{\text{CPET}}^\ddagger$ ) as a fit function for the experimental data in Figure 7, one extracts  $\Delta G_{\text{CPET}}^\ddagger = 5.0 \pm 0.6 \text{ kcal/mol}$ . The activation enthalpy amounts to  $\Delta H_{\text{CPET}}^\ddagger = 2.6 \pm 0.4 \text{ kcal/mol}$ , and the activation entropy is  $\Delta S_{\text{CPET}}^\ddagger = -8.1 \pm 0.9 \text{ cal K}^{-1} \text{ mol}^{-1}$ .

In the framework of the adiabatic Marcus equation, barriers and rate constants are governed by only two parameters, namely, the reorganization energy ( $\lambda_{\text{CPET}}$ ) and reaction free energy ( $\Delta G_{\text{CPET}}^0$ ). This Marcus treatment predicts that  $\Delta \Delta G_{\text{CPET}}^\ddagger / \Delta \Delta G_{\text{CPET}}^0 = 0.5 + \Delta G_{\text{CPET}}^0 / 2\lambda_{\text{CPET}}$ , where  $\Delta G_{\text{CPET}}^\ddagger$  is the activation free energy. Linear regression fits to the data in Figure 6 (excluding the yellow data point for 4-cyanophenol in Figure 6a) yield slopes ( $\Delta \Delta G_{\text{CPET}}^\ddagger / \Delta \Delta G_{\text{CPET}}^0$ ) of  $0.52 \pm 0.05$  for bidirectional and  $0.37 \pm 0.05$  for unidirectional CPET, respectively. The finding that both of these slopes are close to 0.5 is compatible with CPET reactions that take place with low driving forces, in particular with  $-\Delta G_{\text{CPET}}^0 \ll \lambda_{\text{CPET}}/2$ .<sup>28</sup> Given a maximal free energy of  $-0.4 \text{ eV}$  (see above), it would appear then that  $\lambda_{\text{CPET}} > 0.8 \text{ eV}$  ( $18.5 \text{ kcal/mol}$ ) in our systems. In the adiabatic version of Marcus theory, when  $\Delta G_{\text{CPET}}^0$  is close to zero, the reorganization energy ( $\lambda_{\text{CPET}}$ ) is nearly twice the value of  $\Delta G_{\text{CPET}}^\ddagger$ . The lowest



$\Delta G_{\text{CPET}}^0$  for the termolecular reactions from Scheme 1b is expected for Br-PhOH (CN-PhOH does not appear to react predominantly via CPET, see above). On the basis of  $k_{\text{CPET}} = (4.99 \pm 0.41) \times 10^6 \text{ M}^{-1} \text{ s}^{-1}$  for Br-PhOH (Table 3), one finds  $\Delta G_{\text{CPET}}^\ddagger = 5.9 \pm 0.6 \text{ kcal/mol}$  and  $\lambda_{\text{CPET}} = 11.8 \pm 1.2 \text{ kcal/mol}$ . Prior studies of bidirectional CPET with hydrogen-bonded phenols reported reorganization energies  $>22 \text{ kcal/mol}$ .<sup>15,29</sup>

## SUMMARY AND CONCLUSIONS

Bidirectional and unidirectional CPET involving two chemically very closely related sets of reactants (Scheme 1) exhibit very similar driving-force dependence of reaction rates. This strongly supports the concept of thermodynamic equivalence between separated electron/proton acceptors ( $\text{Ru}((\text{CF}_3)_2\text{bpy})_3^{2+}$ , pyridine) and single-reagent hydrogen atom acceptors ( $\text{Ru}(\text{bpz})_3^{2+}$ ).<sup>6</sup> Several prior studies have confirmed the usefulness of this concept,<sup>8,24</sup> but the systems from Scheme 1 are special in that the reactants used for unidirectional and bidirectional PCET are as similar as possible. This permits a direct comparison of the two different reaction types.

In principle one might expect bi- and unidirectional CPET to be associated with substantially different reorganization energies, but in the driving-force range considered here such effects do not clearly manifest.

## EXPERIMENTAL SECTION

$\text{Ru}((\text{CF}_3)_2\text{bpy})_3^{2+}$  was synthesized following a previously reported method.<sup>6</sup> The phenols are commercially available.  $^1\text{H}$  NMR spectra were measured in  $\text{CD}_3\text{CN}$  at  $22^\circ\text{C}$  using a Bruker Avance 400 MHz spectrometer. For deuteration, the phenols were stirred in  $\text{CD}_3\text{OD}$  (99.8% isotope purity) under  $\text{N}_2$  at  $25^\circ\text{C}$  for 1 h. Then the solvent was evaporated, and the whole procedure was repeated once more. For the measurements of the deuterated phenols, acetonitrile and pyridine were predried over  $3 \text{ \AA}$  molecular sieves and then distilled after heating to reflux for 15 min over  $\text{CaH}_2$ . Dry pyridine and  $\text{CH}_3\text{CN}$  were stored over  $3 \text{ \AA}$  molecular sieves under nitrogen atmosphere. Steady-state luminescence spectroscopy occurred on a Fluorolog 3 instrument from Horiba Jobin-Yvon; the excitation wavelength was 450 nm. Time-resolved luminescence and transient absorption studies were conducted on a LP920 KS instrument from Edinburgh Instruments using the frequency-doubled output (532 nm) of a Quantel Brilliant b  $\text{Nd}^{3+}$ :YAG laser for excitation. The pulse duration was  $\sim 10 \text{ ns}$ . Luminescence decays were detected at 610 nm. The  $\text{Ru}((\text{CF}_3)_2\text{bpy})_3^{2+}$  concentration in the luminescence experiments was  $2 \times 10^{-5} \text{ M}$ ; the phenol and pyridine concentrations were as indicated in the individual figure captions. The transient absorption measurements occurred by time-integration over a period of  $5 \mu\text{s}$  starting  $2 \mu\text{s}$  after excitation. The  $\text{Ru}((\text{CF}_3)_2\text{bpy})_3^{2+}$  concentration in the transient absorption experiments was  $7 \times 10^{-5} \text{ M}$ , and the phenol and pyridine concentrations were 0.1–0.5 and 1.0 M, respectively.

## ASSOCIATED CONTENT

### Supporting Information

Additional optical spectroscopic data, including quenching data, luminescence data, transient absorption spectra;  $^1\text{H}$  NMR titration data, derivation of eq 3, estimation of BDFEs for  $\text{CH}_3\text{CN}$  solution, error calculation, temperature-dependence studies. This material is available free of charge via the Internet at <http://pubs.acs.org>.

## AUTHOR INFORMATION

### Corresponding Author

\*E-mail: [oliver.wenger@unibas.ch](mailto:oliver.wenger@unibas.ch).

## Author Contributions

The manuscript was written through contributions of all authors. All authors have given approval to the final version of the manuscript.

## Notes

The authors declare no competing financial interest.

## ACKNOWLEDGMENTS

This work was funded by the Swiss National Science Foundation through Grant No. 200021\_146231/1.

## REFERENCES

- (1) Weinberg, D. R.; Gagliardi, C. J.; Hull, J. F.; Murphy, C. F.; Kent, C. A.; Westlake, B. C.; Paul, A.; Ess, D. H.; McCafferty, D. G.; Meyer, T. J. *Chem. Rev.* **2012**, *112*, 4016.
- (2) (a) Mayer, J. M. *Annu. Rev. Phys. Chem.* **2004**, *55*, 363. (b) Hammes-Schiffer, S.; Stuchebrukhov, A. A. *Chem. Rev.* **2010**, *110*, 6939.
- (3) Bordwell, F. G.; Cheng, J. P. *J. Am. Chem. Soc.* **1991**, *113*, 1736.
- (4) Matsuo, T.; Mayer, J. M. *Inorg. Chem.* **2005**, *44*, 2150.
- (5) (a) Biczok, L.; Gupta, N.; Linschitz, H. *J. Am. Chem. Soc.* **1997**, *119*, 12601. (b) Rhile, I. J.; Mayer, J. M. *J. Am. Chem. Soc.* **2004**, *126*, 12718. (c) Magnuson, A.; Berglund, H.; Korall, P.; Hammarström, L.; Åkermark, B.; Styring, S.; Sun, L. C. *J. Am. Chem. Soc.* **1997**, *119*, 10720. (d) Concepcion, J. J.; Brennaman, M. K.; Deyton, J. R.; Lebedeva, N. V.; Forbes, M. D. E.; Papanikolas, J. M.; Meyer, T. J. *J. Am. Chem. Soc.* **2007**, *129*, 6968. (e) Lachaud, T.; Quaranta, A.; Pellegrin, Y.; Dorlet, P.; Charlot, M. F.; Un, S.; Leibl, W.; Aukauloo, A. *Angew. Chem., Int. Ed.* **2005**, *44*, 1536. (f) Moore, G. F.; Hambourger, M.; Gervald, M.; Poluektov, O. G.; Rajh, T.; Gust, D.; Moore, T. A.; Moore, A. L. *J. Am. Chem. Soc.* **2008**, *130*, 10466. (g) Pizano, A. A.; Yang, J. L.; Nocera, D. G. *Chem. Sci.* **2012**, *3*, 2457. (h) Shukla, D.; Young, R. H.; Farid, S. J. *Phys. Chem. A* **2004**, *108*, 10386. (i) Bonin, J.; Costentin, C.; Robert, M.; Savéant, J. M. *Org. Biomol. Chem.* **2011**, *9*, 4064. (j) Salamone, M.; Amorati, R.; Menichetti, S.; Viglianisi, C.; Bietti, M. *J. Org. Chem.* **2014**, *79*, 6196. (k) Cape, J. L.; Bowman, M. K.; Kramer, D. M. *J. Am. Chem. Soc.* **2005**, *127*, 4208. (l) Sun, L. C.; Burkitt, M.; Tamm, M.; Raymond, M. K.; Abrahamsson, M.; LeGourriérec, D.; Frapart, Y.; Magnuson, A.; Kenéz, P. H.; Brandt, P.; Tran, A.; Hammarström, L.; Styring, S.; Åkermark, B. *J. Am. Chem. Soc.* **1999**, *121*, 6834. (m) Hammarström, L.; Styring, S. *Energy Environ. Sci.* **2011**, *4*, 2379. (n) Johansson, O.; Wolpher, H.; Borgström, M.; Hammarström, L.; Bergquist, J.; Sun, L. C.; Åkermark, B. *Chem. Commun.* **2004**, 194. (o) Costentin, C.; Robert, M.; Savéant, J. M.; Tard, C. *Acc. Chem. Res.* **2014**, *47*, 271. (p) Roth, J. P.; Yoder, J. C.; Won, T. J.; Mayer, J. M. *Science* **2001**, *294*, 2524. (q) Megiatto, J. D.; Mendez-Hernandez, D. D.; Tejeda-Ferrari, M. E.; Teillout, A. L.; Llansola-Portoles, M. J.; Kodis, G.; Poluektov, O. G.; Rajh, T.; Mujica, V.; Groy, T. L.; Gust, D.; Moore, T. A.; Moore, A. L. *Nat. Chem.* **2014**, *6*, 423. (r) Eisenhart, T. T.; Dempsey, J. L. *J. Am. Chem. Soc.* **2014**, *136*, 12221.
- (6) Waidmann, C. R.; Miller, A. J. M.; Ng, C. W. A.; Scheuermann, M. L.; Porter, T. R.; Tronic, T. A.; Mayer, J. M. *Energy Environ. Sci.* **2012**, *5*, 7771.
- (7) (a) Bronner, C.; Wenger, O. S. *J. Phys. Chem. Lett.* **2012**, *3*, 70. (b) Wenger, O. S. *Acc. Chem. Res.* **2013**, *46*, 1517.
- (8) Warren, J. J.; Tronic, T. A.; Mayer, J. M. *Chem. Rev.* **2010**, *110*, 6961.
- (9) Furue, M.; Maruyama, K.; Oguni, T.; Naiki, M.; Kamachi, M. *Inorg. Chem.* **1992**, *31*, 3792.
- (10) Yamaji, M.; Oshima, J.; Hidaka, M. *Chem. Phys. Lett.* **2009**, *475*, 235.
- (11) Kütt, A.; Leito, I.; Kaljurand, I.; Soovali, L.; Vlasov, V. M.; Yagupolskii, L. M.; Koppel, I. A. *J. Org. Chem.* **2006**, *71*, 2829.
- (12) Isuzu, K. *Acid-Base Dissociation Constants in Dipolar Aprotic Solvents*; Blackwell Scientific Publications: Oxford, U.K., 1990.

- (13) (a) Warren, J. J.; Mayer, J. M. *Proc. Natl. Acad. Sci. U. S. A.* **2010**, *107*, 5282. (b) dos Santos, R. M. B.; Simoes, J. A. M. *J. Phys. Chem. Ref. Data* **1998**, *27*, 707.
- (14) Biczók, L.; Linschitz, H. *J. Phys. Chem.* **1995**, *99*, 1843.
- (15) Rhile, I. J.; Markle, T. F.; Nagao, H.; DiPasquale, A. G.; Lam, O. P.; Lockwood, M. A.; Rotter, K.; Mayer, J. M. *J. Am. Chem. Soc.* **2006**, *128*, 6075.
- (16) Das, P. K.; Encinas, M. V.; Steenken, S.; Scaiano, J. C. *J. Am. Chem. Soc.* **1981**, *103*, 4162.
- (17) Lind, J.; Shen, X.; Eriksen, T. E.; Merenyi, G. *J. Am. Chem. Soc.* **1990**, *112*, 479.
- (18) Macomber, R. S. *J. Chem. Educ.* **1992**, *69*, 375.
- (19) (a) Abraham, M. H.; Grellier, P. L.; Prior, D. V.; Duce, P. P.; Morris, J. J.; Taylor, P. J. *J. Chem. Soc., Perkin Trans. 2* **1989**, 699. (b) Snelgrove, D. W.; Luszyk, J.; Banks, J. T.; Mulder, P.; Ingold, K. U. *J. Am. Chem. Soc.* **2001**, *123*, 469.
- (20) (a) Chen, J.; Kuss-Petermann, M.; Wenger, O. S. *Chem.—Eur. J.* **2014**, *20*, 4098. (b) Chen, J.; Kuss-Petermann, M.; Wenger, O. S. *J. Phys. Chem. B* **2015**, *119*, 2263.
- (21) Markle, T. F.; Rhile, I. J.; Mayer, J. M. *J. Am. Chem. Soc.* **2011**, *133*, 17341.
- (22) (a) Migliore, A.; Polizzi, N. F.; Therien, M. J.; Beratan, D. N. *Chem. Rev.* **2014**, *114*, 3381. (b) Zhang, M.-T.; Irebo, T.; Johansson, O.; Hammarström, L. *J. Am. Chem. Soc.* **2011**, *133*, 13224.
- (23) Kaljurand, I.; Kütt, A.; Soovali, L.; Rodima, T.; Maemets, V.; Leito, I.; Koppel, I. A. *J. Org. Chem.* **2005**, *70*, 1019.
- (24) Tarantino, K. T.; Liu, P.; Knowles, R. R. *J. Am. Chem. Soc.* **2013**, *135*, 10022.
- (25) Murov, S. L.; Carmichael, I.; Hug, G. L. *Handbook of photochemistry*, 2nd ed.; Marcel Dekker Inc.: New York, 1993.
- (26) Evans, M. G.; Polanyi, M. *Trans. Faraday Soc.* **1938**, *34*, 0011.
- (27) We also estimated the activation free energy from temperature-dependence studies (see below) and found these estimates to be associated with relative errors of 11%. The errors associated with our activation free energy estimates, which are based on  $k_{\text{CPET}}$  measurements at a single temperature, are therefore assumed to be associated with errors on the order of 11% as well.
- (28) Mayer, J. M. *Acc. Chem. Res.* **1998**, *31*, 441.
- (29) Schrauben, J. N.; Cattaneo, M.; Day, T. C.; Tenderholt, A. L.; Mayer, J. M. *J. Am. Chem. Soc.* **2012**, *134*, 16635.